

Evidence for coronal temperature variation in Seyfert 2 ESO 103–035 using *NuSTAR* observations

SAMUZAL BARUA,¹ V. JITHESH,^{2,3} RANJEEV MISRA,² GULAB C DEWANGAN,² RATHIN SARMA,⁴ AMIT PATHAK,⁵ AND
BIMAN J MEDHI¹

¹*Department of Physics, Gauhati University, Jalukbari, Guwahati-781014, Assam, India*

²*Inter-University Centre for Astronomy and Astrophysics (IUCAA), PB No.4, Ganeshkhind, Pune-411007, India*

³*Department of Physics, University of Calicut, Malappuram-673635, Kerala, India*

⁴*Department of Physics, Rabindranath Tagore University, Hojai-782435, Assam, India*

⁵*Department of Physics, Banaras Hindu University, Varanasi-221005, India*

ABSTRACT

We report flux-resolved spectroscopic analysis of the active galactic nucleus (AGN) ESO 103–035 using *NuSTAR* observations. Following an earlier work, we fit the spectra using a thermal Comptonization model with a relativistic reflection component to obtain estimates of the coronal temperature for two flux levels. The coronal temperature was found to increase from $24.0^{+6.8}_{-3.4}$ to $55.3^{+54.6}_{-7.2}$ keV (errors at 1- σ confidence level) as the flux increased from 9.8 to 11.9×10^{-11} erg cm⁻² s⁻¹ in the 3–78 keV band. A marginal variation in the high energy photon index allows for both, a non-varying optical depth and for the optical depth to have varied by a factor of ~ 2 . This is in contrast to a previous work on *NuSTAR* flux resolved spectroscopy of the AGN, Ark 564, where the temperature was found to decrease with flux along with a 10% variation in the optical depth. The results maybe understood in a framework where AGN variability is either dominated by coronal heating variation leading to correlated increase of temperature with flux and the opposite effect being seen when the variability is dominated by changes in the seed photon flux.

Keywords: Black hole physics (159) — Active galaxies (17) — X-ray active galactic nuclei (2035) — Seyfert galaxies (1447) — High energy astrophysics(739)

1. INTRODUCTION

Strong and rapid variation in the X-ray emission is one of the foremost characteristics of active galactic nuclei (AGN; McHardy & Czerny 1987; Lawrence & Papadakis 1993; Green et al. 1993; Fabian 1999; Nandra 2001; Boller et al. 2003). AGN host a super-massive black hole (SMBH; Peterson 1997; Fabian 1999; Beckmann & Shrader 2012), which powers the activity through accretion of matter (Salpeter 1964; Lynden-Bell 1969; Rees 1984), at a rate sometimes close to the Eddington limit (Fabian 1999).

The hard X-ray emission from AGN is a consequence of inverse-Compton scattering of soft photons from an accretion disk around the SMBH by hot thermal electrons in a corona located above the disk (Sunyaev & Truemper 1979; Haardt & Maraschi 1993; Merloni &

Fabian 2003). The X-ray emission sometimes strike the optically thick accretion disk and gets reflected, resulting in an iron K-line emission peaked at around 6–7 keV and a Compton reflection hump beyond ~ 20 keV (e.g. George & Fabian 1991). Furthermore, these reflection features get modified by the effects of strong gravity.

The coronal temperature, in principle, can be determined by fitting broadband X-ray spectrum using Comptonization and reflection components. Nevertheless, until recently, it was challenging to conduct such measurements due to the low sensitivity of the detectors at high energies and the complexities that arise while the fitting a relativistically blurred reflection component.

However, these difficulties have been overcome by data from *Nuclear Spectroscopic Telescope Array (NuSTAR)*; Harrison et al. 2013), which has X-ray detectors operating in 3–79 keV energy range. Using focusing optics, *NuSTAR* provides an angular resolution (FWHM) of 18", and has a spectral resolution (FWHM) of 0.4 and 0.9 keV at 10 and 60 keV, respectively. It is sen-

Table 1. Fitted parameters from the time-averaged *NuSTAR* FPMA and FPMB spectra

N_H (10^{22} cm $^{-2}$)	Γ	A_{Fe} (solar)	kT_e (keV)	$\log\xi$ [log(erg cm s $^{-1}$)]	θ (degree)	R	R_{in} (r_g)	Norm (10^{-4})	$F_{3-78\text{ keV}}$ (10^{-11} erg cm $^{-2}$ s $^{-1}$)	χ_r^2 /d.o.f
$16.2^{+0.59}_{-0.53}$	$1.73^{+0.02}_{-0.02}$	$0.99^{+0.14}_{-0.13}$	$20.20^{+2.88}_{-1.83}$	$2.80^{+0.07}_{-0.08}$	< 17	$0.18^{+0.01}_{-0.01}$	$24.43^{+6.02}_{-3.16}$	$1.77^{+0.09}_{-0.07}$	$9.89^{+0.03}_{-0.03}$	0.96/1291
$15.96^{+0.56}_{-0.34}$	$1.79^{+0.03}_{-0.02}$	–	$32.53^{+7.63}_{-4.15}$	$2.12^{+0.08}_{-0.19}$	–	$0.29^{+0.07}_{-0.05}$	–	$1.91^{+0.06}_{-0.04}$	$10.47^{+0.03}_{-0.03}$	–

NOTE—The spectra from both ~ 27 ks and ~ 42 ks observations are fitted jointly using `relxill1Cp` model in 3–78 keV band. The model includes absorption using `zTBABS`. From left to right the model parameters are: intrinsic absorption (N_H), photon index (Γ), iron abundance (A_{Fe}), temperature of coronal electrons (kT_e), log of the ionization parameter (ξ), inclination of the accretion disk (θ), reflection fraction (R), the inner disk radius (R_{in}), normalization, unabsorbed 3–78 keV flux ($F_{3-78\text{ keV}}$) and reduced χ^2 with degrees of freedom. The first row lists the free parameters from the ~ 27 ks data, while the second row lists the parameters for the ~ 42 ks data. The inclination, iron abundance and inner disk radius are tied between the two observations.

sitive enough to make a $3\text{-}\sigma$ detection in a 10^6 s exposure of a source with flux $\sim 2(\sim 10) \times 10^{-15}$ erg cm $^{-2}$ s $^{-1}$ in the 6–10 (10–30) keV band (Harrison et al. 2013). As demonstrated by Garca et al. (2015), these specifications are sufficient for determining the high-energy cut-off, which in turn allows one to measure the coronal temperature through spectral fitting. Indeed, *NuSTAR* observations of a number of AGN have provided the opportunity to determine their corona temperature. For a number of AGNs, the high energy cut-off has been estimated using *NuSTAR* data as listed in Table 1 of Fabian et al. (2015). These high energy cut-offs can then be used to estimate the coronal temperature (e.g. Middei et al. 2019) which in turn allows for testing whether pair-production is important for these systems or not (Fabian et al. 2015). For a thermal plasma, there is a maximum threshold temperature beyond which a pair cascade would occur and this threshold depends on the compactness parameter $l = L\sigma_T/Rm_e c^3$, where L is the luminosity and R is the size of the corona (Svensson 1984; Zdziarski 1985). The estimated temperatures for some of the sources are close to the pair-production threshold value, which suggests that the temperature is perhaps being regulated by pair production. The inclusion of non-thermal electrons in the corona decreases the pair production threshold temperature, and thus the sources with cooler temperatures may also be regulated by the same mechanism (Fabian et al. 2017). Correlation between the cut-off energy and spectral index over long time-scales have been reported (e.g. Zoghbi et al. 2017; Tortosa et al. 2018). Direct temperature measurements have been made, for example for 3C 382 (Ballantyne et al. 2014), but these were typically at high values (> 100 keV). Recently, there have been reports of direct measurement of low coronal temperatures in AGN. The AGN Ark 564 was found to have a temperature of ~ 15 keV (Kara et al. 2017). Temperature estimates have been reported for

a few other AGN, ESO 103–035 ($kT_e \sim 22$ keV), IGR 2124.7+5058 ($kT_e \sim 20$ keV; Buisson et al. 2018, hereafter B18), 2MASS J1614346+470420 ($kT_e \sim 45$ keV) and B1422+231 ($kT_e \sim 28$ keV; Lanzuisi et al. 2019).

AGN variability is observed in flux and continuum shape changes which are sometimes correlated. Analysing such variability in detail, provides physical insight into the AGN. One of the important variability behavior that has been observed in both AGN and X-ray binaries, is that the spectral index of the X-ray continuum correlates with the soft X-ray flux (Haardt et al. 1997; Zdziarski et al. 2003; Sobolewska & Papadakis 2009). The X-ray continuum steepens as the source flux increases which could be a consequence of inverse-Comptonization process (Zdziarski et al. 2003). Since radiative cooling is efficient, the corona should be continuously heated via some phenomenon so as to sustain it at a high temperature (Fabian et al. 2015). Now, if the input soft photon flux increases, the radiative cooling of the corona becomes more effective and in case the heating rate is a constant, the coronal temperature should naturally decrease. If the optical depth of the corona remains the same, such a decrease in the temperature would result in hardening of the spectrum and hence this may explain the steepening of the spectrum as the flux increases. Until recently, there were only indirect ways to infer that the coronal temperature indeed varies with flux. For example, Wilkins & Gallo (2015) inferred the change in temperature by showing that the corona has undergone an expansion.

In Barua et al. (2020), we performed flux resolved spectroscopy of *NuSTAR* data of the AGN Ark 564, and showed that the coronal temperature decreased with increasing flux. Furthermore, the variation was accompanied by an increase in optical depth. ESO 103–035 is another suitable AGN that belongs to the class of Seyfert 2 type, whose *NuSTAR* data provides the opportunity to test the variation of coronal temperature

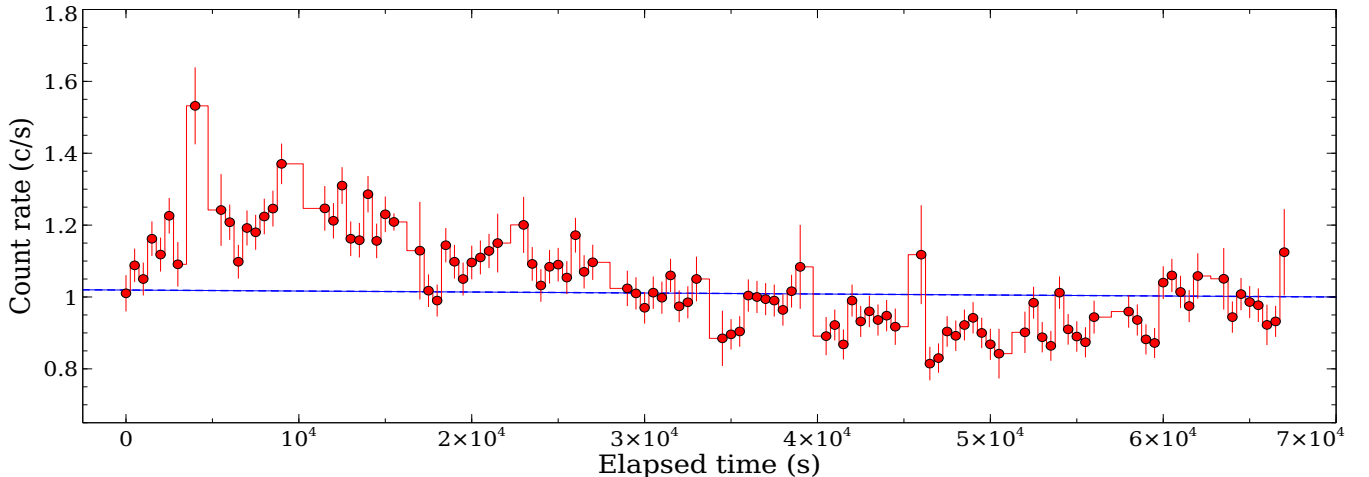


Figure 1. The ~ 42 ks *NuSTAR* light curve of ESO 103–035 extracted with a bin size of 500 s. The blue dotted horizontal line divides the light curve into two flux states, low: 0–1.02 c/s and high: 1.02–1.6 c/s flux states.

with flux. Recently, B18 have analyzed 3–78 keV X-ray spectra of ESO 103–035 using two *NuSTAR* observations conducted in 2013 and 2017, with exposure times of 27.3 and 42.5 ksecs, respectively. The spectral analysis with the *NuSTAR* data provided direct observational evidence for a low-temperature corona, ~ 22 keV in ESO 103–035.

ESO 103–035 ($z = 0.0133 \pm 0.0003$; Phillips et al. 1979) was discovered as a powerful source of X-ray emission with HEAO-A2 (Marshall et al. 1979; Piccinotti et al. 1982). The X-ray spectrum of ESO 103–035 revealed a strong iron $K\alpha$ line (Wilkes et al. 2001) along with some absorption features (Phillips et al. 1979). From the *BeppoSAX* observation in 1996, Akylas et al. (2001) reported a spectral index of ~ 1.87 , and an iron emission line peaked at 6.4 keV with a width of 0.3 ± 0.1 keV. In the *BeppoSAX* observation, the continuum spectrum could be described by a power law with a high energy cut-off at 29 ± 10 keV (Wilkes et al. 2001). This observation also revealed that the source is highly absorbed with a column density $N_H = 1.79 \pm 0.09 \times 10^{23}$ cm^{-2} . The timing properties of the source (i.e. the shape of the power density spectrum) provided a black hole mass estimate of $M_{BH} = 10^{7.1 \pm 0.6} M_\odot$ (Czerny et al. 2001).

In this work, we re-analyze the 27.3 ks and 42.5 ks *NuSTAR* observations to investigate the flux dependent spectral variability of Seyfert 2 ESO 103–035. In §2, we describe the observation used and data reduction. In §3, we present the results of the spectral fitting analysis and discuss the results in §4.

2. OBSERVATION AND DATA REDUCTION

The *NuSTAR* satellite observed the Seyfert 2 ESO 103–035 in 2013 and 2017 for exposure of 27.3 ks (Ob-

servation ID:60061288002) and 42.5 ks (Observation ID: 60301004002), respectively. The source has also been observed by *Swift*, simultaneously to both *NuSTAR* observations. However, the *Swift* exposure times are short, ~ 6.8 ks and ~ 2 ks for the ~ 27 ks and ~ 42 ks of *NuSTAR* data sets, respectively. These short exposure data are insufficient for flux resolved analysis and hence we have not used the *Swift* data. The *NuSTAR* data processed with *NuSTAR* data analysis pipeline (NUPipeline) in order to produce calibrated and filtered data products. For this standard pipeline processing, we used *NuSTAR* data analysis software (NUS-TARDAS) v1.8.0 and CALDB version 20171002. From the cleaned event files, all required final products such as light curves, spectra were extracted using NUPRODUCTS script. We extracted a circular source region with a 60 arcsec radius and a larger circular background region with a 90 arcsec radius that was away from the source region (as used in B18). SAA filtering was applied using “saacalc=2 saamode=optimized tentacle=yes”. The extracted regions for both the source as well as background were the same for two *NuSTAR* instruments, Focal Plane Module A and Focal Plane Module B (FPMA and FPMB). The FPMA and FPMB spectra were grouped using the GRPPHA tool so as to have 50 counts in each spectral bin.

3. SPECTRAL FITTING

3.1. Time-averaged spectrum

We first re-analysed the time averaged spectra of the two observations as has been done by B18. While, B18 fitted the spectra with different physical models, here we focus only on the thermal Comptoniza-

tion model with a relativistic reflection `relxillCp`¹, since we are interested in estimating the coronal temperature. This model assumes that primary component is due to inverse-Comptonization represented by the XSPEC model `nthComp` (Zdziarski et al. 1996; Życki et al. 1999). Additionally, we use the absorption model `zTBABS` (Wilms et al. 2000) to account for the intrinsic absorption in the source. We estimate the errors and the confidence contours using the Markov chain Monte Carlo (MCMC) analysis for which we use the XSPEC_EMCEE code developed by Jeremy Sanders² (Sanders & Fabian 2013), which is a Python implementation of Goodman & Weare’s Affine Invariant Markov chain Monte Carlo (MCMC) Ensemble sampler. We use the default number of walkers 50 with 15000 iterations each, then burned the first 1000 in order to estimate errors from the steady chain. We quote 1- σ errors on best-fit parameters corresponding to 68% confidence level everywhere unless otherwise specified. To take into account possible difference in the effective area of the FPMA and FPMB instruments, a constant multiplier was applied to the model for FPMB spectrum.

We first reproduce the results obtained in B18 by fitting the spectra of the two observations and found that the spectral parameters obtained were consistent with theirs. For the ~ 42 and ~ 27 ksec observation, we obtained the best fit values of the coronal temperature to be $kT_e = 25.9^{+12.4}_{-4.7}$ and $kT_e = 50.2^{+38.4}_{-13.5}$ keV, respectively as compared to 22^{+19}_{-6} and > 20 keV reported by B18. We could also broadly constrain the inner disk radius $R_{in} \sim 25^{+6}_{-8} r_g$ while B18 report and upper limit of $17 r_g$. The slight difference in the parameter ranges could be due to the use of MCMC technique and/or due to the presence of multiple close local minima in the χ^2 space caused by the complexity of the model. Like other Seyfert 2 AGN, a narrow Iron K- α line emission has been reported for the ESO 103–035 (Noguchi et al. 2009; Liu & Wang 2010). However, this emission line is weaker than what is typically observed in Seyfert 1 AGN (Liu & Wang 2010). These may be the reason why here in this work, we do not see any significant improvement in the spectral fitting upon adding a narrow reflection component.

Next, we fitted the spectra from the two observations jointly, keeping the Iron abundance (A_{Fe}), the disc inclination angle (θ) and the inner radius (R_{in}) to have the same values, while allowing for the rest of the free

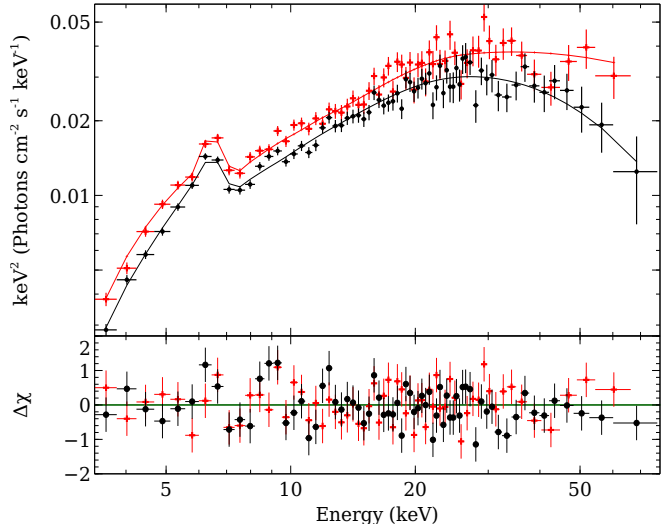


Figure 2. Unfolded *NuSTAR* FPMA spectra of ESO 103–035 from two flux states. The black circles and red plus represent the low and high flux states, respectively. These spectra are fitted with `relxillCp` model.

parameters to vary independently. This is physically reasonable since these parameters are not expected to vary. The best-fit free spectral parameters from the MCMC analysis are listed in Table 1. The spectral fitting is rather insensitive to the other parameters of the model which describes the reflection component (B18) and hence were fixed at nominal values i.e. the outer radius to $400 r_g$, the emissivity index to 3 and the spin of the black hole to 0.99.

This joint fitting allows for a better constrain on the electron temperature for both observations. The estimated temperatures are constrained to be at $20.2^{+2.9}_{-1.8}$ and $32.5^{+7.6}_{-4.2}$ keV, for the 27 ks and 42 ks observations, respectively. In the joint fit, some other parameters like the Iron abundance are also better constrained, however the best fit values are roughly similar to the ones obtained by the individual fits and by B18.

3.2. Flux-resolved spectra

To study the flux dependent coronal temperature variation in ESO 103–035, we obtained flux-resolved spectra by splitting the 42.5 ks *NuSTAR* observation into two different flux states, which are denoted here as low and high flux states. These low and high flux states consisted of data when the count rate was in the range 0–1.02 c/s and 1.02–1.6 c/s, respectively as shown in Figure 1. This resulted in the high (low) flux state to have an exposure of ~ 16 ksec (~ 27 ksec) and total counts of ~ 13300 (~ 18500). The ~ 27 ks observation of ESO 103–035 does not exhibit significant flux variation in the light curve

¹ <http://www.sternwarte.uni-erlangen.de/~dauser/research/relxill/>

² https://github.com/jeremysanders/xspec_emcee

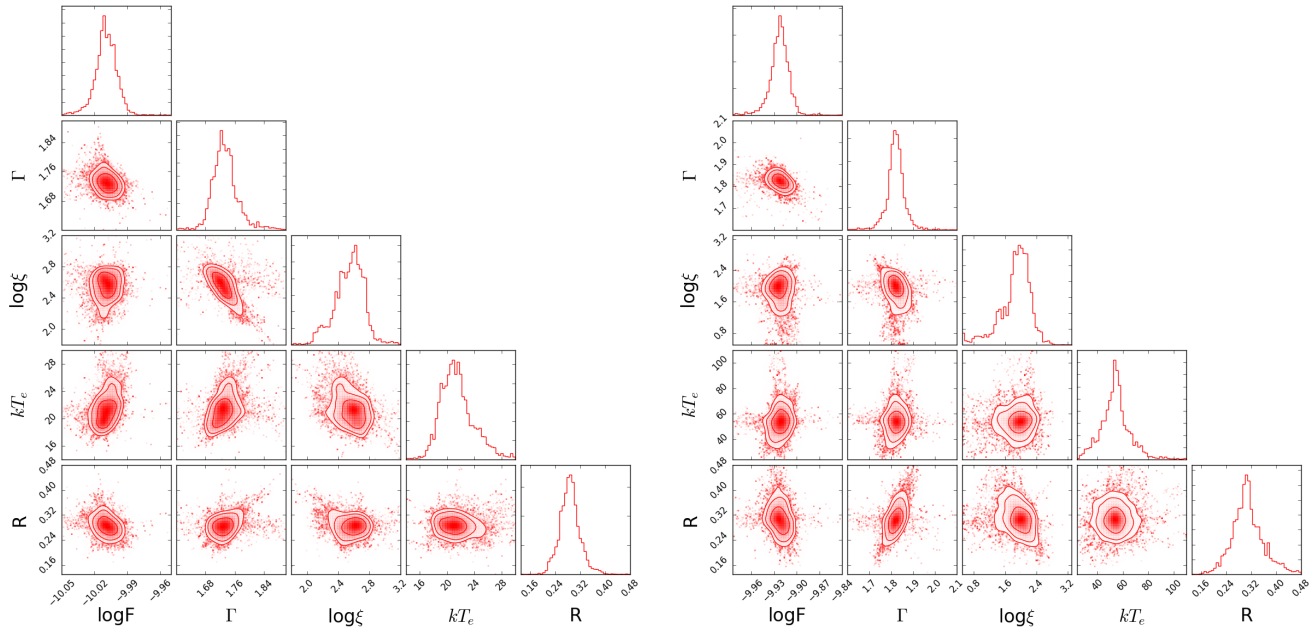


Figure 3. Corner plots of spectral parameters obtained from the analysis of flux-resolved spectra. The left and right hand panels represent MCMC results for low and high flux states, respectively.

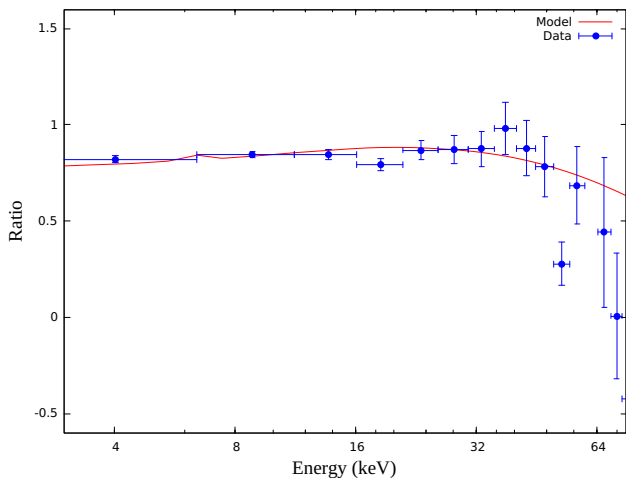


Figure 4. The ratio of the *NuSTAR* data from the low and high flux states. The blue circles represent the ratio of the spectra from high to low flux states, whereas the red line represents the model ratio of the same.

(see Figure 1 of B18), and hence was not considered for flux-resolved spectroscopy.

The average count rates for low and high flux states are 0.674 ± 0.005 and 0.806 ± 0.007 c/s, respectively. Similar to the spectral modeling of the time-averaged spectrum as discussed in the previous section, the 3–78 keV flux-resolved spectra were fitted using the same relativistic reflection model `relxillCp`. The iron abundance (A_{Fe}), Inner disk radius (R_{in}) and the absorption column density were fixed to the values obtained from

the time-averaged spectrum. Also, we fixed the inclination angle (θ) to be 10 degree as it was constrained to be less than 17 degree in the time-averaged analysis. The unfolded spectra and residuals are shown in Figure 2. The unabsorbed flux in the 3–78 keV range was estimated using the XSPEC model `cf1flux` and the free spectral parameters are listed in Table 2. The spectral analysis of these spectra indicates the variation of the coronal electron temperature, which increased from $24.0^{+6.8}_{-3.4}$ to $55.3^{+54.6}_{-7.2}$ keV as the flux increased. This temperature variation is seen to accompanied by a marginal increase of the photon index, from $1.76^{+0.02}_{-0.03}$ to $1.81^{+0.06}_{-0.02}$. In order to examine the degeneracy between the spectral parameters we constructed corner plots from the MCMC analysis and show them in Figure 3. It is seen that though some pairs of parameters show moderate to strong degeneracy still all of them are well constrained. To show the spectral variation in a model independent way, the ratio of the high to low spectra is shown in Figure 4 which indicates a curvature at high energies, implying an increase of the coronal temperature as the flux increases. We further quantify the significance of the coronal temperature variation result by fitting a constant to the two temperature values which gives a χ^2 of 5.25 for one degree of freedom. This implies a null hypothesis probability that the temperatures are same to be less than 0.02 or in other words the result that the temperatures are different is at 98 % confidence level.

We also fitted the high and low flux state spectra joint by keeping the temperature tied, which resulted in a

$\chi^2/\text{dof} = 871.9/923$ as compared to when they were kept free, $\chi^2/\text{dof} = 866.5/921$. An F-test gives the significance of the temperature variation at $\sim 95\%$. Instead of `relxillCp`, if we use `relxill` (which incorporates a cut-off power-law continuum instead of a thermal Comptonization one), the cut-off energy was found to be larger for the high flux state, $69.5_{-11.4}^{+16.6}$ keV as compared to the low flux state, $39.3_{-2.9}^{+4.9}$ keV, providing a supporting evidence to the observed temperature variation. If instead of defining the high and low flux states as having count rate (CR) greater than or less than ~ 1 c/s, we choose ~ 0.98 c/s as the threshold, the best fit temperature of the high state turns out to be $46.2_{-9.0}^{+22.9}$ keV, while it is $21.3_{-1.6}^{+10.2}$ keV for the corresponding low state. For a threshold of ~ 1.1 c/s, the high (low) state temperature turns out to be $103.4_{-3.0}^{+119.8}$ keV ($23.3_{-3.0}^{+6.7}$). Thus, the result that the coronal temperature increases with flux is not very sensitive to the demarking flux level. If instead of two, we consider three flux states, defined as low (CR < 0.98 c/s), medium ($0.98 < \text{CR} < 1.1$ c/s) and high (CR > 1.1 c/s), the best fit temperatures turn out to be $21.3_{-1.6}^{+10.2}$, $34.0_{-7.2}^{+18.0}$ and $103.4_{-11.2}^{+119.8}$ keV, respectively. The best fit temperatures of the two lower flux states are consistent with each other, and hence considering three flux states does not improve the statistical significance of the result. The errors quoted in this work are from the MCMC technique, which may sometimes be different from those obtained using the standard χ^2 variance method. Using the standard method, the temperature estimates for the high and low flux states turn out to be 55_{-16}^{+90} and 24_{-5}^{+7} keV respectively, which although different from the values quoted in Table 2, are consistent with the result, that the temperature increased with flux.

4. DISCUSSION AND CONCLUSION

We have investigated the variability of the coronal temperature of ESO 103–035 using the *NuSTAR* observations. Our study revealed that probably (at > 95% confidence level) the coronal temperature increased by a factor of ~ 2 when the flux increased by $\sim 22\%$. While other spectral did not show any significant variation, the photon index (Γ) increased by roughly 0.1. Using the equation,

$$\tau = \sqrt{\frac{9}{4} + \frac{3}{\theta \left[\left(\Gamma + \frac{1}{2} \right)^2 - \frac{9}{4} \right]}} - \frac{3}{2} \quad (1)$$

where $\theta = kT_e/m_e c^2$, we estimate the optical depth (τ) of the corona to be $3.45_{-0.76}^{+1.34}$ and $1.85_{-0.57}^{+2.98}$ in low and high flux states, respectively. Thus, while the optical

depth is not well constrained a large variation by a factor of two is also consistent. We note that the ~ 27 ksec observation with a flux of $\sim 9.9 \times 10^{-11}$ erg cm $^{-2}$ s $^{-1}$ and coronal temperature estimate of $20.2_{-1.8}^{+2.9}$ keV is consistent with the flux and temperature values obtained for the low flux resolved spectrum.

The results may be contrasted with that found for Ark 564 (Barua et al. 2020), where the coronal temperature was found to *decrease* with increasing flux accompanied by about 10% increase in the optical depth. The different behavior of the two systems can be reconciled by considering that the flux variation in ESO 103–035 is due to changes in the heating rate of the corona, leading to a correlated variation of the coronal temperature and flux. On the other hand, for Ark 564, the flux variation could be driven by variation in the input seed photon flux, leading to the expected anti-correlation between temperature and flux. Both variations may well be accompanied by changes in the optical depth of the corona.

It is interesting to note that there is a qualitative difference between the X-ray spectral shapes of Ark 564 and ESO 103–035. While for Ark 564, the high energy photon index is ~ 2.3 that is greater than 2.0, for ESO 103–035 it is $\sim 1.7 < 2.0$. This means that the flux of ESO 103–035 is dominated by emission at high energies ~ 30 keV, while for Ark 564 it is dominated by low energy emission. Thus, flux of ESO 103–035 would be more sensitive to changes in the coronal heating rate than seed photon rate and the vice-versa would hold for Ark 564. This maybe a clue to the reason why the two sources show different correlation of corona temperature with flux.

The results presented here along with the earlier result for Ark 564, suggest that AGN variability could be dominated by either seed photon changes or coronal heating variation, with each process exhibiting a different correlation of the corona temperature with flux. Clearly, the analysis has to be undertaken for a larger number of sources, to draw conclusions regarding which process dominates and whether that depends on the spectral properties of the source. Moreover, even for the same source, the two process could dominate at different times. It is also likely that both coronal heating variation and seed photon flux changes are active at the same time and perhaps can occur with a time difference. Here, one can perhaps draw an analogy with black hole X-ray binaries which also have a hot corona Comptonizing low energy photons, to produce high energy X-ray emission. Detailed variability studies of X-ray binaries have revealed that both the seed photon flux and the coronal heating rate vary and they do so after a time lag which depends on the time-scale of the variation (Maq-

Table 2. Fitted Parameters from the flux-resolved spectra of ESO 103–035 from ~ 42 ks observation

Flux state	Γ	kT_e (keV)	$\log\xi$ [$\log(\text{erg cm s}^{-1})$]	R	Norm (10^{-4})	$F_{3-78 \text{ keV}}$ ($10^{-11} \text{ erg cm}^{-2} \text{ s}^{-1}$)	χ_r^2 /d.o.f
1 (Low)	$1.76_{-0.03}^{+0.02}$	$24.04_{-3.42}^{+6.80}$	$2.31_{-0.06}^{+0.09}$	$0.31_{-0.02}^{+0.06}$	$1.66_{-0.07}^{+0.10}$	$9.76_{-0.04}^{+0.04}$	0.95/527
2 (High)	$1.81_{-0.02}^{+0.06}$	$55.3_{-7.2}^{+54.6}$	$2.17_{-0.33}^{+0.15}$	$0.28_{-0.04}^{+0.08}$	$2.29_{-0.05}^{+0.18}$	$11.87_{-0.04}^{+0.04}$	0.93/395

NOTE—The spectral fitting is done similar to the fits of time-averaged spectrum. The iron abundance (A_{Fe}), inner disk radius (R_{in}) and column density (N_H) parameters are fixed to the values obtained from the analysis of the time-averaged spectrum, while the inclination angle (θ) is fixed at 10 degree.

bool et al. 2019; Jithesh et al. 2019; Mudambi et al. 2020; Jithesh et al. 2021). Flux resolved spectroscopy using sensitive instruments like *NuSTAR* for a larger sample of AGN with more continuous monitoring, will reveal the nature of the variability of these sources.

We thank the anonymous referee for the constructive comments and suggestions that improved this manuscript. SB acknowledges the IUCAA Visiting program. SB, RS & RM acknowledge the SERB research grant EMR/2016/005835. This research has made use of data obtained from the High Energy Astrophysics Science Archive Research Center (HEASARC), provided by NASA’s Goddard Space Flight Center, and the *NuSTAR* Data Analysis Software (NUSTARDAS) jointly developed by the ASI Science Data Center (ASDC, Italy) and the California Institute of Technology (Caltech, USA).

Facilities: NuSTAR

Software: XSPEC, EMCEE (Sanders & Fabian 2013), NUSTARDAS,

REFERENCES

- Akylas, A., Georgantopoulos, I., & Comastri, A. 2001, Monthly Notices of the Royal Astronomical Society, 324, 521, doi: [10.1046/j.1365-8711.2001.04375.x](https://doi.org/10.1046/j.1365-8711.2001.04375.x)
- Ballantyne, D. R., Bollenbacher, J. M., Brenneman, L. W., et al. 2014, ApJ, 794, 62, doi: [10.1088/0004-637X/794/1/62](https://doi.org/10.1088/0004-637X/794/1/62)
- Barua, S., Jithesh, V., Misra, R., et al. 2020, Monthly Notices of the Royal Astronomical Society, 492, 3041, doi: [10.1093/mnras/staa067](https://doi.org/10.1093/mnras/staa067)
- Beckmann, V., & Shrader, C. R. 2012
- Boller, T., Voges, W., Dennefeld, M., et al. 2003, A&A, 397, 557, doi: [10.1051/0004-6361:20021520](https://doi.org/10.1051/0004-6361:20021520)
- Buisson, D. J. K., Fabian, A. C., & Lohfink, A. M. 2018, Monthly Notices of the Royal Astronomical Society, 481, 4419, doi: [10.1093/mnras/sty2609](https://doi.org/10.1093/mnras/sty2609)
- Czerny, B., Nikolajuk, M., Piasecki, M., & Kuraszkiwicz, J. 2001, MNRAS, 325, 865, doi: [10.1046/j.1365-8711.2001.04522.x](https://doi.org/10.1046/j.1365-8711.2001.04522.x)
- Fabian, A. C. 1999, Proceedings of the National Academy of Sciences, 96, 4749, doi: [10.1073/pnas.96.9.4749](https://doi.org/10.1073/pnas.96.9.4749)
- Fabian, A. C., Lohfink, A., Belmont, R., Malzac, J., & Coppi, P. 2017, MNRAS, 467, 2566, doi: [10.1093/mnras/stx221](https://doi.org/10.1093/mnras/stx221)
- Fabian, A. C., Lohfink, A., Kara, E., et al. 2015, Monthly Notices of the Royal Astronomical Society, 451, 4375, doi: [10.1093/mnras/stv1218](https://doi.org/10.1093/mnras/stv1218)
- García, J. A., Dauser, T., Steiner, J. F., et al. 2015, The Astrophysical Journal, 808, L37, doi: [10.1088/2041-8205/808/2/137](https://doi.org/10.1088/2041-8205/808/2/137)
- George, I. M., & Fabian, A. C. 1991, Monthly Notices of the Royal Astronomical Society, 249, 352, doi: [10.1093/mnras/249.2.352](https://doi.org/10.1093/mnras/249.2.352)
- Green, A. R., McHardy, I. M., & Lehto, H. J. 1993, MNRAS, 265, 664, doi: [10.1093/mnras/265.3.664](https://doi.org/10.1093/mnras/265.3.664)
- Haardt, F., & Maraschi, L. 1993, ApJ, 413, 507, doi: [10.1086/173020](https://doi.org/10.1086/173020)
- Haardt, F., Maraschi, L., & Ghisellini, G. 1997, The Astrophysical Journal, 476, 620, doi: [10.1086/303656](https://doi.org/10.1086/303656)

- Harrison, F. A., Craig, W. W., Christensen, F. E., et al. 2013, *The Astrophysical Journal*, 770, 103, doi: [10.1088/0004-637x/770/2/103](https://doi.org/10.1088/0004-637x/770/2/103)
- Jithesh, V., Maqbool, B., Misra, R., et al. 2019, *ApJ*, 887, 101, doi: [10.3847/1538-4357/ab4f6a](https://doi.org/10.3847/1538-4357/ab4f6a)
- Jithesh, V., Misra, R., Maqbool, B., & Mall, G. 2021, *MNRAS*, 505, 713, doi: [10.1093/mnras/stab1307](https://doi.org/10.1093/mnras/stab1307)
- Kara, E., García, J. A., Lohfink, A., et al. 2017, *MNRAS*, 468, 3489, doi: [10.1093/mnras/stx792](https://doi.org/10.1093/mnras/stx792)
- Lanzuisi, G., Gilli, R., Cappi, M., et al. 2019, *ApJL*, 875, L20, doi: [10.3847/2041-8213/ab15dc](https://doi.org/10.3847/2041-8213/ab15dc)
- Lawrence, A., & Papadakis, I. 1993, *ApJL*, 414, L85, doi: [10.1086/187002](https://doi.org/10.1086/187002)
- Liu, T., & Wang, J.-X. 2010, *ApJ*, 725, 2381, doi: [10.1088/0004-637X/725/2/2381](https://doi.org/10.1088/0004-637X/725/2/2381)
- Lynden-Bell, D. 1969, *Nature*, 223, 690, doi: [10.1038/223690a0](https://doi.org/10.1038/223690a0)
- Maqbool, B., Mudambi, S. P., Misra, R., et al. 2019, *MNRAS*, 486, 2964, doi: [10.1093/mnras/stz930](https://doi.org/10.1093/mnras/stz930)
- Marshall, F. E., Boldt, E. A., Holt, S. S., et al. 1979, *ApJS*, 40, 657, doi: [10.1086/190600](https://doi.org/10.1086/190600)
- McHardy, I., & Czerny, B. 1987, *Nature*, 325, 696, doi: [10.1038/325696a0](https://doi.org/10.1038/325696a0)
- Merloni, A., & Fabian, A. C. 2003, *Monthly Notices of the Royal Astronomical Society*, 342, 951, doi: [10.1046/j.1365-8711.2003.06600.x](https://doi.org/10.1046/j.1365-8711.2003.06600.x)
- Middei, R., Bianchi, S., Marinucci, A., et al. 2019, *A&A*, 630, A131, doi: [10.1051/0004-6361/201935881](https://doi.org/10.1051/0004-6361/201935881)
- Mudambi, S. P., Maqbool, B., Misra, R., et al. 2020, *ApJL*, 889, L17, doi: [10.3847/2041-8213/ab66bc](https://doi.org/10.3847/2041-8213/ab66bc)
- Nandra, K. 2001, *Advances in Space Research*, 28, 295, doi: [10.1016/S0273-1177\(01\)00409-4](https://doi.org/10.1016/S0273-1177(01)00409-4)
- Noguchi, K., Terashima, Y., & Awaki, H. 2009, *ApJ*, 705, 454, doi: [10.1088/0004-637X/705/1/454](https://doi.org/10.1088/0004-637X/705/1/454)
- Peterson, B. M. 1997
- Phillips, M. M., Feldman, F. R., Marshall, F. E., & Wamsteker, W. 1979, *A&A*, 76, L14
- Piccinotti, G., Mushotzky, R. F., Boldt, E. A., et al. 1982, *ApJ*, 253, 485, doi: [10.1086/159651](https://doi.org/10.1086/159651)
- Rees, M. J. 1984, *ARA&A*, 22, 471, doi: [10.1146/annurev.aa.22.090184.002351](https://doi.org/10.1146/annurev.aa.22.090184.002351)
- Salpeter, E. E. 1964, *ApJ*, 140, 796, doi: [10.1086/147973](https://doi.org/10.1086/147973)
- Sanders, J. S., & Fabian, A. C. 2013, *MNRAS*, 429, 2727, doi: [10.1093/mnras/sts543](https://doi.org/10.1093/mnras/sts543)
- Sobolewska, M. A., & Papadakis, I. E. 2009, *Monthly Notices of the Royal Astronomical Society*, 399, 1597, doi: [10.1111/j.1365-2966.2009.15382.x](https://doi.org/10.1111/j.1365-2966.2009.15382.x)
- Sunyaev, R. A., & Truemper, J. 1979, *Nature*, 279, 506, doi: [10.1038/279506a0](https://doi.org/10.1038/279506a0)
- Svensson, R. 1984, *MNRAS*, 209, 175, doi: [10.1093/mnras/209.2.175](https://doi.org/10.1093/mnras/209.2.175)
- Tortosa, A., Bianchi, S., Marinucci, A., Matt, G., & Petrucci, P. O. 2018, *A&A*, 614, A37, doi: [10.1051/0004-6361/201732382](https://doi.org/10.1051/0004-6361/201732382)
- Wilkes, B. J., Mathur, S., Fiore, F., Antonelli, A., & Nicastro, F. 2001, *ApJ*, 549, 248, doi: [10.1086/319063](https://doi.org/10.1086/319063)
- Wilkins, D. R., & Gallo, L. C. 2015, *Monthly Notices of the Royal Astronomical Society*, 449, 129, doi: [10.1093/mnras/stv162](https://doi.org/10.1093/mnras/stv162)
- Wilms, J., Allen, A., & McCray, R. 2000, *ApJ*, 542, 914, doi: [10.1086/317016](https://doi.org/10.1086/317016)
- Zdziarski, A. A. 1985, *ApJ*, 289, 514, doi: [10.1086/162912](https://doi.org/10.1086/162912)
- Zdziarski, A. A., Johnson, W. N., & Magdziarz, P. 1996, *Monthly Notices of the Royal Astronomical Society*, 283, 193, doi: [10.1093/mnras/283.1.193](https://doi.org/10.1093/mnras/283.1.193)
- Zdziarski, A. A., Lubiński, P., Gilfanov, M., & Revnivtsev, M. 2003, *Monthly Notices of the Royal Astronomical Society*, 342, 355, doi: [10.1046/j.1365-8711.2003.06556.x](https://doi.org/10.1046/j.1365-8711.2003.06556.x)
- Zoghbi, A., Matt, G., Miller, J. M., et al. 2017, *ApJ*, 836, 2, doi: [10.3847/1538-4357/aa582c](https://doi.org/10.3847/1538-4357/aa582c)
- Życki, P. T., Done, C., & Smith, D. A. 1999, *MNRAS*, 309, 561, doi: [10.1046/j.1365-8711.1999.02885.x](https://doi.org/10.1046/j.1365-8711.1999.02885.x)